Materials Today Physics 29 (2022) 100919

Contents lists available at ScienceDirect

Materials Today Physics

journal homepage: www.journals.elsevier.com/materials-today-physics

Near-infrared responsive gecko-inspired flexible arm gripper

Xiaohang Luo [a,1], Xiaoxiao Dong [b,c,1], Hong Zhao [b,***], Travis Shihao Hu [d], Xiuping Lan [a], Lan Ding [a], Jiapeng Li [a], Huiqin Ni [a,e], Jordan A. Contreras [d], Hongbo Zeng [c,**], Quan Xu [a,*]

[a] State Key Laboratory of Heavy Oil Processing, China University of Petroleum (Beijing), Beijing, 102249, China
[b] College of Mechanical Transportation Engineering, China University of Petroleum (Beijing), Beijing, 102249, China
[c] Department of Chemical and Materials Engineering, University of Alberta, Edmonton, Alberta, T6G 1H9, Canada
[d] Department of Mechanical Engineering, California State University, Los Angeles, CA, 90032, USA
[e] Department of Applied Physics, Aalto University, P.O. BOX 11000(Otakaari 1B), Helsiniki, FI00076, AALTO, Finland

ARTICLE INFO

Keywords:
Gecko
dry adhesives
Infrared-responsive
Hydrogel
PDMS
Flexible arm gripper
Gradient

ABSTRACT

Inspired by the microstructure of gecko toes, a drivable bionic gecko toe adhesion surface with double-layer structure was designed and fabricated. The driving ability is derived from the volume shrinkage of the dehydrated hydrogel after the driving hydrogel layer is irradiated by near-infrared light (808 nm) (the temperature of the single-layer hydrogel can be increased from 17.9 °C to 107 °C within 30s, and the curling angle can be curled by 0°–180°, similar to the folded state.), and another layer with a microstructure similar to gecko toes can withstand a maximum shear force of 22.4N/cm^{-2}. The different properties of the two layers are combined together to achieve a reversible transition of adhesion/desorption similar to the gecko walking process. The double-layer structure of the drivable bionic gecko toe adhesion surface was structurally optimized to prepare a four-arm gripper that could grasp/release only by unilateral irradiation. This bilayer-structured bionic gecko toe adhesion surface has great design potential, and in the future, it is hoped that it can provide insights into the preparation of large-actuated remote-controlled robots and fast-actuated soft robots.

1. Introduction

Mother nature keep stimulating new innovations in science and engineering at an accelerated pace [1–5]. Among them, geckos have received continuous attention for decades by virtue of their special toepads with strong adhesion, easy detachemnt, and self-cleaning properties [6–13]. It is well known that the geckos can run quickly in almost all surfaces, and the evidences have shown that the adhesion performance of gecko toe is attributed to the accumulation of 'secondary' intermolecular forces (e.g., van der Waals forces) [14,15]. Using the above properties can create products with strong adhesion, such as tapes, wall climbing tires, etc. It is worth noting that the research on the reversible transformation that can achieve automatic grasp-release in response to an external field and preserve the adhesion and detachment properties of gecko toes is not yet mature. Therefore, we consider trying to connect the optimized adhesion layer with the actuation layer corresponding to the external environment to prepare a double-layered biomimetic surface with both adhesion and environmental response characteristics.

About the optimization of the traditional gecko toe adhesive layer to achieve better performance, Dong et al. found that the proteins in a single gecko seta exhibit gradient distribution characteristics and the Young's modulus of each individual seta gradually decreases from the proximal to distal direction along the setal stalk. It's worth mentioning that the distribution of protein and Young's modulus in the seta are all in a gradient distribution state. It is proven that the gradient distribution is beneficial to improve the robustness and service life of the seta verified by both experiments and simulations [16]. Wang incorporated 15 wt% Fe_3O_4 nanoparticle coated with SiO_2 core-shell structure (Fe_3O_4@SiO_2) into poly(urethane acrylate) (PUA), and prepared gecko-inspired

* Corresponding author.
** Corresponding author.
*** Corresponding author.
E-mail addresses: 15603641616@163.com (X. Luo), 2849754958@qq.com (X. Dong), hzhao_cn@163.com (H. Zhao), shu17@calstatela.edu (T.S. Hu), 15770707817@163.com (X. Lan), 15030527652@163.com (L. Ding), 18811744699@163.com (J. Li), 15110194113@163.com (H. Ni), jcontr61@calstatela.edu (J.A. Contreras), hongbo.zeng@ualberta.ca (H. Zeng), xuquan@cup.edu.cn (Q. Xu).
[1] Xiaohang Luo and Xiaoxiao Dong are the co-first authors.

https://doi.org/10.1016/j.mtphys.2022.100919
Received 22 July 2022; Received in revised form 31 October 2022; Accepted 14 November 2022
Available online 16 November 2022

slanted functional gradient pillars (s-FGPs). The gradient distribution of Fe_3O_4@SiO_2 in PUA is achieved by combining template assisted UV curing method. The s-FGPs surface showed decent firmness, durability, anisotropy and roughness adaptability [17]. Inspired by the strong adhesive properties of geckos and tree frogs, Liu et al. prepared a T-shape gradient micropillars (TG) biomimetic surface with stiff tip and soft root. $CaCO_3$ nanoparticles were dispersed in poly(dimethylsiloxane) (PDMS) the micropillars in a gradient form by a centrifugation method. It is demonstrated that the TG surface is beneficial to the contact formation and removal, so that the adhesion and friction force are increased by 4.6 and 2.4 times, respectively, compared with pure PDMS pillars without gradient change in modulus [18].

About the ability to reversibly transform the adhesion and desorption of the imitation gecko toe adhesive layer, such as factors that respond to light, electricity, and magnetic fields. In the previous work research, Xu and co-workers added 2,2,6,6-Tetramethylpiperidinooxy (TEMPO)-doped PDA, modified MoO_3, and carbon dots, respectively, to the PDMS based gecko-like toe-adhesion surfaces to achieve response to NIR/UV. These material systems achieve temperature control by light irradiation of specific wavelengths, thereby affecting the adhesion properties of the biomimetic surfaces [19,20]. In addition, Zhou et al. grafted polymers on silicon nanowires. The attachment and detachment are chemically triggered (e.g., PH, electrolyte solution), and by humidity [21]. More recently, Zhou et al. have successfully developed a self-peeling switchable dry/wet adhesive (SPSA), combining the gecko-inspired microstructure and the mussel-inspired surface chemistry. The prepared SPSA realize a self-peeling process by incorporating Fe_3O_4 nanoparticles into the pillars for thermal-responsive control, which is effective in air and/or underwater [22].

Herein, we step further and combine a hydrogel system with Fe_3O_4 nanoparticle gradient doping PDMS-based surface to prepare a new generation type of gecko-like toe surface. We utilized a hydrogel system (poly(acrylamide-co-N-isopropyl acrylamide-*co*-tannic acid)-Fe [named as p(AAm-*co*-NIPAAm-*co*-TA)-Fe]) combined with an optimized gecko-like paw layer (gradient Fe_3O_4/poly(dimethylsiloxane) [named as GFe/PDMS]). And a fast and flexible near-infrared light-controlled gripper with grasping and releasing is prepared. The proposed design principles and structures can be easily applied to the fabrication of similar bionic gecko surfaces, and the new generation of bionic surfaces is expected to be used in some extreme conditions, such as aerospace satellite waste, biochips et al.

2. Results and discussion

The schematic of the reversible adhesion in gecko toe pad is shown in Fig. 1a. The biomimetic surface of gradient Fe_3O_4 magnetic nanoparticles doped in PDMS matrix was prepared by template assisted method (in Fig. 1b), here we refer to this bionic surface as GFe/PDMS for short [16]. The diameter and height of each individual pillars are about 10 μm and 15 μm, respectively. The distance between the centers of each pillar is roughly 15 μm. Scanning electron microscope (SEM) microstructure images and element distribution of GFe/PDMS are shown in Fig. 1c. It can be seen that the micropillar arrays are evenly distributed (Fig. 1c–i). The energy dispersive X-Ray spectroscopy (EDX mapping)

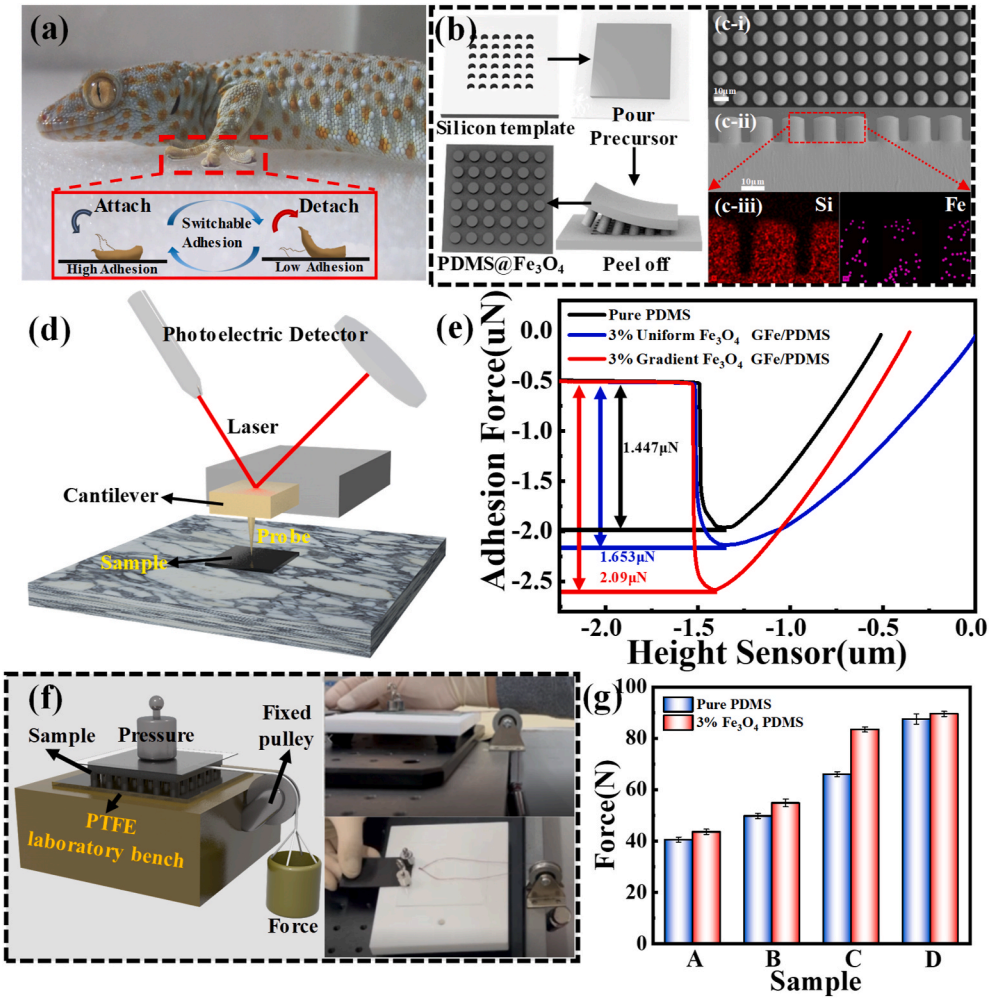

Fig. 1. (a) The reversible adhesion properties schematic diagram of the gecko toe pad, (b) schematics the GFe/PDMS processing, (c) images of cured pattern and elemental mapping: (i) SEM image of the part of the GFe/PDMS surface; (ii) SEM image of a single pillar; (iii) EDX images of the pillar, showing a gradient distribution of the magnetic particles, (d) Schematic of the AFM mechanical properties (adhesion tests) of various samples, (e) The adhesion data of pillar on different biomimetic surfaces, (f) Setup for measuring the macroscopic level shear adhesion of the biomimetic surfaces (pillar arrays: 4 cm by 4 cm in size), (g) Shear force testing of biomimetic surfaces of different sizes and types (The diameter of the micropillars of all samples is 10 μm, the center spacing and length of the micropillars of samples A, B, C, D are 25 μm, 15 μm; 25 μm, 20 μm; 15 μm, 15 μm; 15 μm, 20 μm respectively).

images of one row of pillars are shown in shown in Fig. 1c–ii and c-iii. The element mapping of the pillars shows a uniform distribution of the silicon, while the iron element (corresponding to the Fe_3O_4 magnetic particles) displays a gradient distribution along the pillar longitudinal axis. We compared PDMS micropillar adhesive layer doped with 1 wt%, 2 wt%, 3 wt%, 5 wt%, 7 wt% and 10 wt% Fe_3O_4 magnetic particles. With small amount of doping all magnetic particle may be redistributed to completely concentrate to the bottom or base the micropillars under the applied magnetic field, resulting in no magnetic particles in the man part of the micropillars. Excessive doping of magnetic particles will deteriorate the mechanical properties of PDMS by affecting the crosslinking density of the PDMS (Fig. S1). It was also observed in the experiments that excessive magnetic particles would considerably affect the gelation of PDMS. The optimized doping concentration was identified as 3 wt% of Fe_3O_4 magnetic particles to prepare biomimetic micropillar surfaces. The adhesion of the pillar was measured with an Atomic Force Microscope (AFM), as shown in Fig. 1d. We conducted AFM micromechanical tests on the surface of pure PDMS, PDMS with uniform distribution of 3 wt% Fe_3O_4 nanoparticles, and GFe/PDMS with gradient distribution of 3 wt% Fe_3O_4 nanoparticles. The results show that the GFe/PDMS has the strongest adhesion, 44% higher than that of pure PDMS biomimetic micropillar arrays (in Fig. 1e). We tested various samples on a smooth class surface using a conventional method, where a moderate preloading of 0.2 N/cm^2 was applied in the normal direction [16]. The shear loading was then applied to the various samples and gradually increased until sliding occurred (in Fig. 1f). The shear force test results show that the pure PDMS biomimetic surface can withstand a shear force of 66.06 N, and the GFe/PDMS with a gradient distribution of 3 wt% Fe_3O_4 can withstand a shear force of 83.4 N. We compared the effect of the center distance and length between different pillars on the shear force of biomimetic microarrays surface with the fixed pillar diameter of 10 μm. Regarding the pillar spacing, we find that the shear force of the micro-pillars with a distance of 15 μm is generally higher than that of 25 μm, where the difference between the pure PDMS and PFG surfaces are close to 70% and 76%, respectively. Comparing the shear force of micropillars with lengths of 15 μm and 20 μm, it is found that the biomimetic surface of the pillar with a longer length will generate a stronger shear force, which is more obvious in the pure PDMS surface, with a difference of about 29%, while the difference in GFe/PDMS is about 14%. In addition, the shear force generated on the surface of GFe/PDMS is generally about 12% stronger than that of pure PDMS (in Fig. 1g). Previous studies indicate the gradient distribution of Fe_3O_4 nanoparticles enhances adhesion properties and service life [16].

Strong adhesion and friction forces have been reported for conventional biomimetic gecko micropillar arrays. However, it mostly passive and lack of an active driving mechanism or control. To this end, we have designed a hydrogel p(AAm-*co*-NIPAAm-*co*-TA)-Fe with robust and infrared responsive properties, which is intended to be combined with GFe/PDMS as a driving layer to prepare a new generation of bilayers biomimetic surface. SEM characterization showed that poly(acrylamide-*co*-*N*-isopropyl acrylamide) [named p(AAm-*co*-NIPAAm)], poly(acrylamide-*co*-*N*-isopropyl acrylamide-*co*-tannic acid) [named p(AAm-*co*-NIPAAm-*co*-TA)] and p(AAm-*co*-NIPAAm-*co*-TA)-Fe were homogeneous with uniform porous structures (in Fig. S2). In order to investigate the effect of introducing the Fe on light responsive ness, p(AAm-*co*-NIPAAm), p(AAm-*co*-NIPAAm-*co*- TA) and p(AAm-*co*-NIPAAm-*co*-TA)-Fe are studied and compared. The preparation method and ratio are shown in the experimental section Table 1. To demonstrate the successful preparation of NIR-responsive hydrogels, we performed various characterizations of p(AAm-*co*-NIPAAm-*co*-TA)-Fe. Fourior transform infrared spectroscopy (FTIR) characterization shows that the hydroxyl functional group peak appears at 3300 cm^{-1}, and the hydroxyl peak assumes a blue-shift before and after iron ion treatment (in Fig. 2a), which may be due to the reduction tendency of the oxygen in the phenolic hydroxyl group in tannic acid (TA). The chelation of Fe^{3+} and TA is the key to p(AAm-*co*-NIPAAm-*co*-TA)-Fe response to infrared. To

Table 1
Various experimental materials to prepare prescursor solution.

Name	Dosage/wt%					
	AAm	NIPAAm	BIS	Irga2959	TA	Fe^{3+} mol/L
PAN	5	5	0.25	0.25	2	0.5
p(AAm-*co*-NIPAAm-*co*-TA)	5	5	0.25	0.25	2	0.5
5 wt% p(AAm-*co*-NIPAAm-*co*-TA)-Fe	5	5	0.25	0.25	2	0.5
15 wt% p(AAm-*co*-NIPAAm-*co*-TA)-Fe	5	15	0.25	0.25	2	0.5
25 wt% p(AAm-*co*-NIPAAm-*co*-TA)-Fe	5	25	0.25	0.25	2	0.5
0.5 wt%BIS p(AAm-*co*-NIPAAm-*co*-TA)-Fe	5	5	0.5	0.25	2	0.5
0.75 wt%BIS p(AAm-*co*-NIPAAm-*co*-TA)-Fe	5	5	0.75	0.25	2	0.5
1 wt%BIS p(AAm-*co*-NIPAAm-*co*-TA)-Fe	5	5	1	0.25	2	0.5
0.05 mol/L Fe p(AAm-*co*-NIPAAm-*co*-TA)-Fe	5	5	0.25	0.25	2	0.05
0.25 mol/L Fe p(AAm-*co*-NIPAAm-*co*-TA)-Fe	5	5	0.25	0.25	2	0.25

The wt% represents the content of AAm, NIPAAm, TA, BIS, Irga2959 in 10 g water.

prove that p(AAm-*co*-NIPAAm-*co*-TA)-Fe can achieve chelation after soaking in $FeCl_3$ solution, Raman spectroscopy was perfomed, which shows that two obvious vibration peaks of phenolic hydroxyl Fe^{3+} appeared at 600 cm^{-1} and 670 cm^{-1} [23–25] indicating that Fe^{3+} were successfully chelated in p(AAm-*co*-NIPAAm-*co*-TA) to form p(AAm-*co*--NIPAAm-*co*-TA)-Fe (in Fig. 2b). X-ray photoelectron spectroscopy characterization (XPS) shows that the peaks at 711.5 and 724.8 eV can be attributed to Fe^{3+}, suggesting Fe^{3+} exist in the form of trivalent state (in Fig. S3) [26–28]. The hydrogel changed from transparent to black when it was immersed in $FeCl_3$ solution. (in Fig. S4). Therefore, we tested the UV–Vis diffuse reflection spectroscopy (UV–Vis DRS) and found that the absorption intensity of p(AAm-*co*-NIPAAm-*co*-TA)-Fe was higher than that of p(AAm-*co*-NIPAAm-*co*-TA) and p(AAm-*co*-NIPAAm) in the range of 350 nm–900nm. In particular, the absorbance at 700 nm–800nm increases nearly 5 folds, which indicates p(AAm-*co*-NIPAAm-*co*-TA)-Fe has excellent absorption of 700 nm–800nm wavelength of light (in Fig. 2c).

Next, we performed photothermal tests on the hydrogel, and the schematic is shown in Fig. 2d. The surface temperature of p(AAm-*co*-NIPAAm-*co*-TA)-Fe increases when irradiated by NIR (808 nm, 4 W/cm^2), which causes the hydrogel to effectively heat up and water removal from the matrix. The effects of various NIPAAm contents (5 wt %, 15 wt% and 25 wt%) on the photothermal effect of p(AAm-*co*-NIPAAm-*co*-TA)-Fe were explored (The crosslinker BIS(N,*N*-Methylenebisacrylamide) and the initiator Irga2959(2-(Hydroxymethyl)-N-Methylbenzamide) were 0.25 wt% and 0.5 wt% respectively. The results show that the drive performance is the best when the NIPAAm content is 5 wt%, and the p(AAm-*co*-NIPAAm-*co*-TA)-Fe can curl up from flat to almost 180° folded state within 30s (in Fig. 2e). In addition, hydrogels not soaked in Fe^{3+} have no NIR driving effect. Through the thermal imaging camera, the data and 5 wt% NIPAAm p(AAm-*co*-NIPAAm-*co*-TA)-Fe surface temperature change with time are shown in Fig. 2e–g. The surface temperature of 5 wt% p(AAm-*co*-NIPAAm-*co*-TA)-Fe can be increased from 17.2 °C to 107 °C in 30 s, while p(AAm-*co*-NIPAAm-*co*-TA) is not affected by the same irradiation. A comparison group was also tested, most notably PAN, which is almost transparent and absorbs little infrared light (in Fig S5 a-i-a-iv and Fig S5 b-i-b-iv). We also conduct experiments on the effect of different N,*N*-Methylenebisacrylamide and

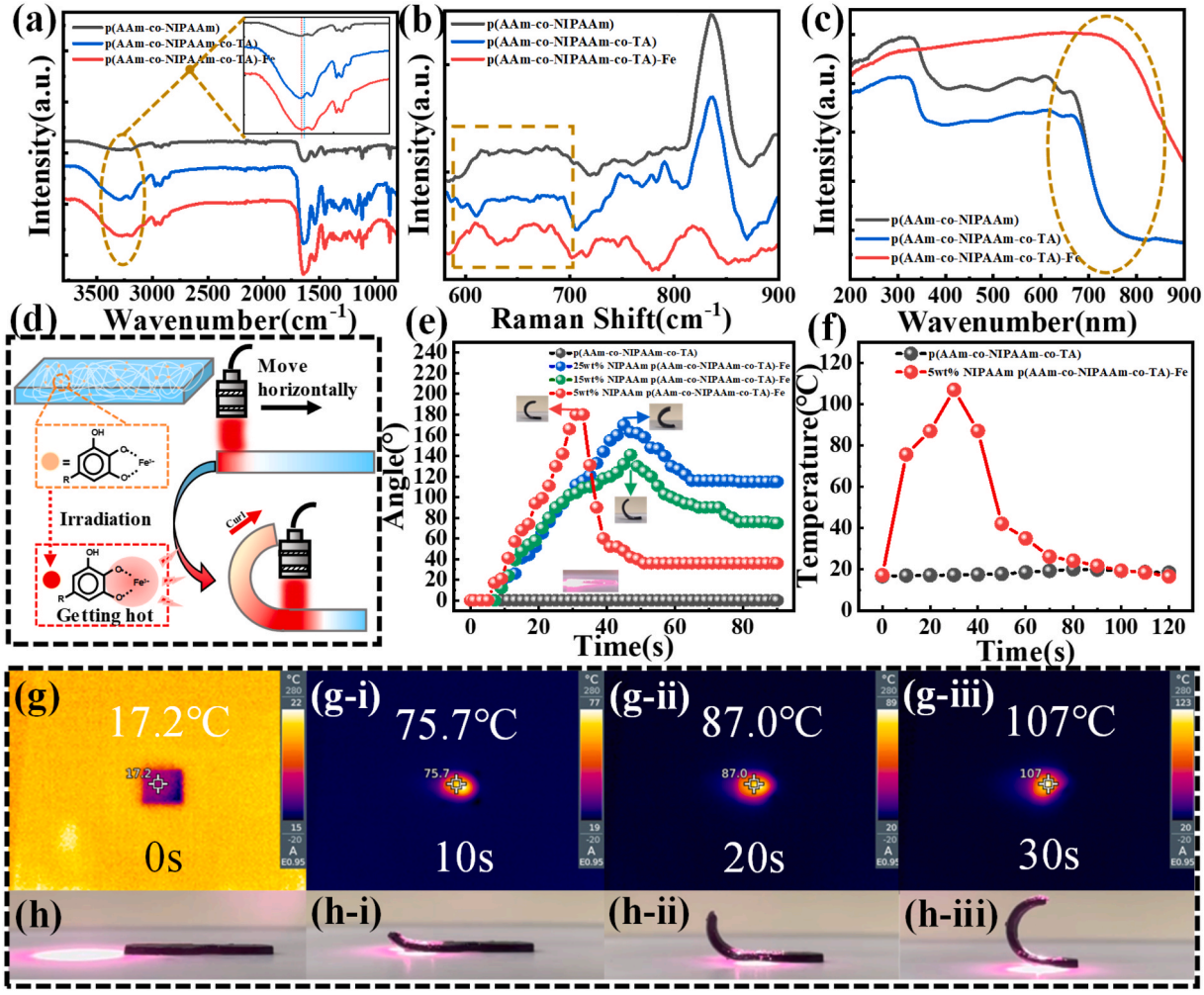

Fig. 2. Characterization tests of p(AAm-*co*-NIPAAm), p(AAm-*co*-NIPAAm-*co*-TA), and p(AAm-*co*-NIPAAm-*co*-TA)-Fe, (a) FTIR, (b) Raman, (c) UV–Vis DRS, (d) Schematic diagram of the infrared driving mechanism of p(AAm-*co*-NIPAAm-*co*-TA)-Fe, (e) The effect of p(AAm-*co*-NIPAAm-*co*-TA)-Fe content on the driving angle, 5 wt% NIPAAm p(AAm-*co*-NIPAAm-*co*-TA)-Fe surface temperature change with infrared irradiation time (f) data graph, (g) pictures, (h) NIR driver diagram of p (AAm-*co*-NIPAAm-*co*-TA)-Fe.

iron ion content on the p(AAm-*co*-NIPAAm-*co*-TA)-Fe infrared driving effect. When other variables are set the same, the driving effect is the best when BIS and iron ion content are 0.025 and 0.5 mol/L, respectively (in Fig. S6 and S7). In addition, we also explored the effects of different wattages of the laser and immersion in aqueous solutions of different pH on the bending angle of the gel. The driving ability of p(AAm-*co*-NIPAAm-*co*-TA)-Fe increases with the laser wattage (in Fig. S8). When the solution is alkaline, Fe^{3+} will dissociate from the phenolic hydroxyl group in the tannic acid, combine with OH^{-}, and Fe^{3+} will permeate the gel; when the solution is acidic, the tannic acid in the phenolic hydroxyl group will first combine with the excess H^{+} in the solution, and as a result, Fe^{3+} will also dissociate from the phenolic hydroxyl group of the tannic acid. Therefore, the gel is not suitable for soaking in high acid or high alkaline solutions (in Fig. S9). The demo of the NIR driving of 5 wt % NIPAAm p(AAm-*co*-NIPAAm-*co*-TA)-Fe is shown in Fig. 2h and Video. 1. It can be seen that p(AAm-*co*-NIPAAm-*co*-TA)-Fe has excellent photothermal performance, which is the basis to prepare the double-layer biomimetic actuation surface of flexible grippers.

Supplementary data related to this article can be found online at https://doi.org/10.1016/j.mtphys.2022.100919

The above-mentioned p(AAm-*co*-NIPAAm-*co*-TA)-Fe is combined with the PDMS biomimetic micropillar arrays, and the preparation procedure is shown in Fig. 3a. By applying an external magnetic field, the Fe_3O_4 in the uncured PDMS matrix can assume a gradient distribution. The as-prepared [p(AAm-*co*-NIPAAm-*co*-TA)-Fe]-*co*-PDMS with gradient distribution was then immersed in benzophenone (BP) solution, to decorate initiator molecular chains on the PDMS surface. There are hydrophilic initiators (Irga2959) in the hydrogel precursors. The hydrophobic initiator (BP) acts as a grafting agent for crosslinking the hydrogel with PDMS, as well as an oxygen scavenger to alleviate oxygen inhibition. The BP acts as a grafting agent for crosslinking the hydrogel with PDMS, as well as an oxygen scavenger to alleviate oxygen inhibition. Meanwhile, the Irga 2959 provide polymerization of hydrogel monomers into hydrogel polymers within and above the surface-bound diffusion layer of the polymer substrates. Furthermore, the insolubility of the BP in water prevents the surface-adsorbed BP from diffusing into the hydrogel pre-gel aqueous solution, effectively limiting the reactions within the surface-bound diffusion layer. This unique combination of selective and defined diffusion of hydrophobic initiators enables the immobilization of hydrogels on PDMS through an interfacial permeation process [29]. Finally, encapsulate the underlying substrate with the imitation gecko toe PDMS layer that has just been soaked, add the p(AAm-*co*-NIPAAm-*co*-TA) precursor solution into the encapsulated mold, cure it under UV light, then open the mold, and soak the cured sample in $FeCl_3$ solution to obtain The double-layer biomimetic surface [p(AAm-*co*-NIPAAm-*co*-TA)-Fe]-PDMS with infrared driving characteristics (Fig. 3b), the specific process refers to the experimental method. We combined pure PDMS and p(AAm-*co*-NIPAAm-*co*-TA)-Fe so that

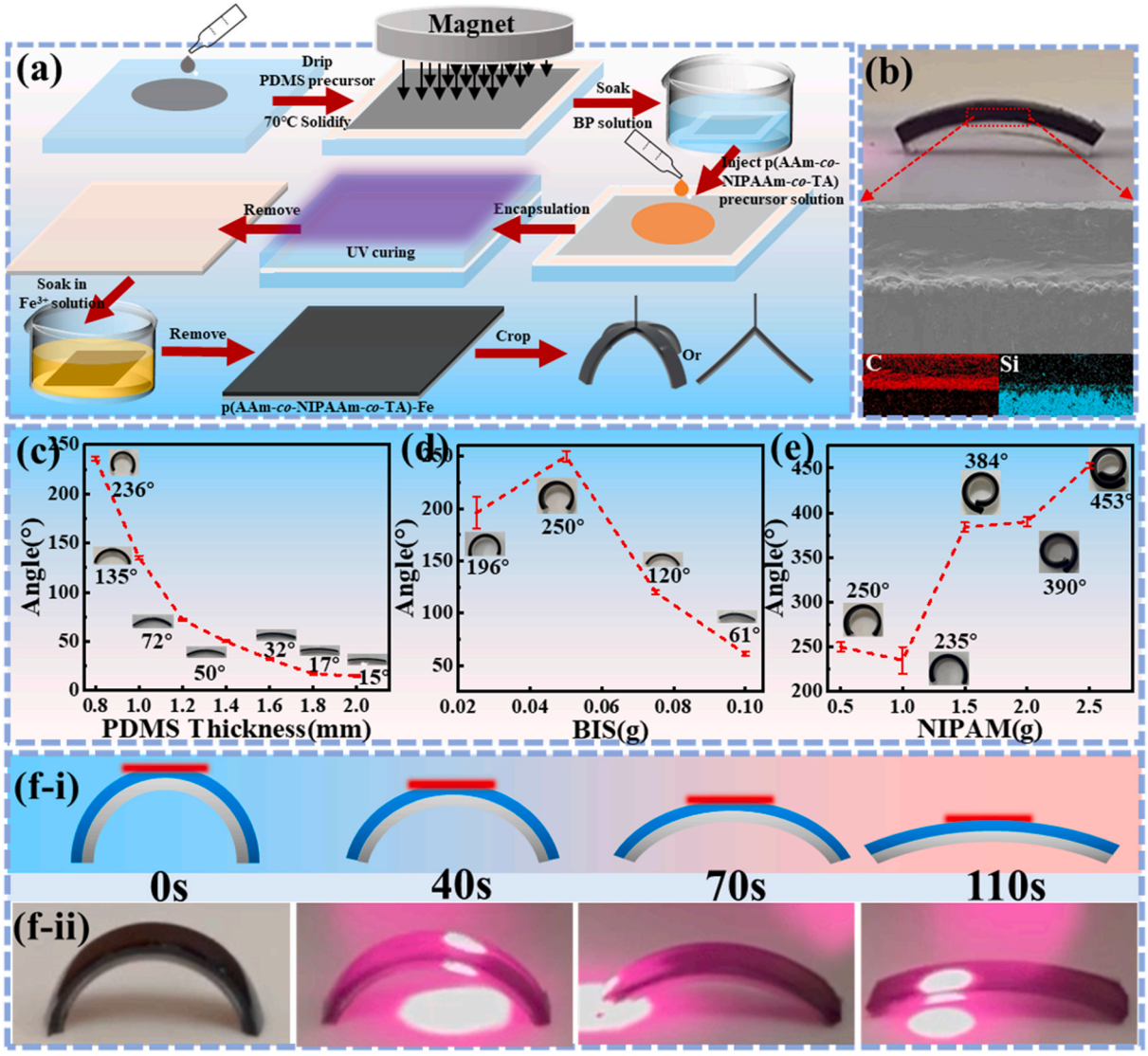

Fig. 3. (a) Schematic diagram of the preparation process of [p(AAm-*co*-NIPAAm-*co*-TA)-Fe]-PDMS, (b) SEM and EDX mapping of the [p(AAm-*co*-NIPAAm-*co*-TA)-Fe]-PDMS, (c–e), Effects of different conditions on the curling angle of [p(AAm-*co*-NIPAAm-*co*-TA)-Fe]-PDMS, (f-i, ii) The infrared drive effect of [p(AAm-*co*-NIPAAm-*co*-TA)-Fe]-PDMS.

there is a clear layer difference when taking pictures. SEM image and EDX mapping illustrate the successful bonding between p(AAm-*co*-NIPAAm-*co*-TA)-Fe and PDMS. The C and Si elements come from p(AAm-*co*-NIPAAm-*co*-TA)-Fe and PDMS, respectively. The Fe element is mainly the $FeCl_3$ solution in p(AAm-*co*-NIPAAm-*co*-TA)-Fe, the reason why there is Fe element in the lower layer may be caused by the scraping of the upper p(AAm-*co*-NIPAAm-*co*-TA)-Fe layer to the surface of the lower layer during cutting.

To understand the swelling effect of p(AAm-*co*-NIPAAm-*co*-TA)-Fe, we explored different amounts of NIPAAm and BIS (when the thickness of PDMS and p(AAm-*co*-NIPAAm-*co*-TA)-Fe were kept the same), and different thicknesses of PDMS with p(AAm-*co*-NIPAAm-*co*-TA)-Fe on the natural curling degree of [p(AAm-*co*-NIPAAm-*co*-TA)-Fe]-PDMS (Fig. 3c–e). As expected, the curling angle of [p(AAm-*co*-NIPAAm-*co*-TA)-Fe]-PDMS decreased gradually with the increase of PDMS layer thickness, and finally approached a near-flat state, and the driving effect also suppressed. With the increase of the amount of BIS, the curling angle of [p(AAm-*co*-NIPAAm-*co*-TA)-Fe]-PDMS firstly increased and then gradually decreased, since BIS would increase the cross-linking sites, thus limiting the swelling effect of p(AAm-*co*-NIPAAm-*co*-TA)-Fe. With the increase of the amount of NIPAAm, the curling angle of [p(AAm-*co*-NIPAAm-*co*-TA)-Fe]-PDMS generally showed an upward trend. We can choose different material ratios according to different actuation requirements. Macroscopically, [p(AAm-*co*-NIPAAm-*co*-TA)-Fe]-PDMS exhibits an arched shape. By irradiating the upper surface of [p(AAm-*co*-NIPAAm-*co*-TA)-Fe]-PDMS with NIR light, the [p(AAm-*co*-NIPAAm-*co*-TA)-Fe]-PDMS gradually flattened and finally assumed a substantially flat state around 110 s (Fig. 3f–i, 3f-ii). This provides the basis for us to design a new type of flexible arm gripper. We used the unbalanced expansion states on both sides of [p(AAm-*co*-NIPAAm-*co*-TA)-Fe]-PDMS to perform object grasping and releasing effect experiments. We designed a dual-arm gripper in Fig. S10a and Video. 2 when the [p(AAm-*co*-NIPAAm-*co*-TA)-Fe]-PDMS on both sides of the dual-arm gripper was in an expanded state, the object can be gripped by the adhesive properties of the PDMS layer. When NIR light hits the outside of the dual-arm gripper, the p(AAm-*co*-NIPAAm-*co*-TA)-Fe layer is driven in response to the infrared light, causing the two arms to extend outward to release the object. To achieve better grasping and releasing effects, we designed a four-arm gripper, which works in the same mechanism as dual-arm gripper (Fig. S10b, Video. 3).

Supplementary data related to this article can be found online at https://doi.org/10.1016/j.mtphys.2022.100919

The flexible arm is bent in the heating direction under the NIR irradiation. The design of the above four-arm gripper has a drawback - the inside of the arm needs to be irradiated with prominent efficiency, and the flexible arm can only grasp objects (as shown in Fig. S10c and Video. 4). However, in actual operation, a specific angle is required to illuminate the inner side, which is difficult to operate. Therefore, we adjusted the four-arm gripper structure (Fig. 4a). The adjusted four-arm gripper divided into three parts: grasping part, releasing part and sticking part. The upper surface of the gripping part is pure PDMS, and the lower surface is p(AAm-*co*-NIPAAm-*co*-TA)-Fe. In the gripping part, the swelling effect of p(AAm-*co*-NIPAAm-*co*-TA)-Fe was suppressed to some extent by PDMS, resulting in a relatively flat surface. When the gripping part is triggered by NIR irradiation, the whole gripper tends to shrink. The adhesive portion utilizes the adhesive properties of the GFe/PDMS surface to improve the grip of the object. There are two routes to release an object. One was placing adjusted four-arm gripper in a humid environment made the p(AAm-*co*-NIPAAm-*co*-TA)-Fe hydrogel absorb water and swell to restore its original shape, thereby releasing the object [30], another was to irradiate the release part of adjusted four-arm gripper, p(AAm-*co*-NIPAAm-*co*-TA)-Fe is affected by infrared rays and will bend outward to release the object. Since the swelling of p(AAm--*co*-NIPAAm-*co*-TA)-Fe with different thicknesses will affect the shape of the gripper (Fig. 3c–e). Moreover, PDMS with different thicknesses also inhibited the driving ability of p(AAm-*co*-NIPAAm-*co*-TA)-Fe to different degrees. Therefore, on the basis of the above two constraints, we designed the PDMS and p(AAm-*co*-NIPAAm-*co*-TA)-Fe layer thicknesses in the grasping part of the adjusted four-arm gripper to be 0.8 mm, 1.2 mm, the sticking part (GFe/PDMS) and the released part thicknesses were 0.8 mm, 1.2 mm, respectively. The process of inward contraction and lateral expansion of adjusted four-arm gripper is shown in Fig. S11 and Video. 5. We tried to use NIR light to remotely control the adjusted four-arm gripper for work, the grasp part of the adjusted four-arm gripper can shrink and grasp the object after about 120s of infrared irrdiation, and the shear force and adhesive force of the adhesion part can keep the object from falling (Fig. 4b-i-4b-v). When infrared continues to irradiate the release part of adjusted four-arm gripper about 60s, p(AAm-*co*-NIPAAm-*co*-TA)-Fe will lose water and bend due to heating, which realizes the release of object (in Fig. 4c-i-4c-v, Video. 6). In contrast, when the adhesive part was replaced by p (AAm-co-NIPAAm-co-TA)-Fe, the flexible arm completely lost its ability to grasp objects. (Fig. S12).

Supplementary data related to this article can be found online at https://doi.org/10.1016/j.mtphys.2022.100919

3. Conclusions

A novel gecko inspired reversible dry adhesive double-layered system which combined the infrared-responsive hydrogel and GFe/PDMS biomimetic surface was successfully proposed to construct. The temperature of optimized hydrogel layer [p(AAm-*co*-NIPAAm-*co*-TA)-Fe] can increase from 17.9 °C to 107 °C under 30 s infrared radiation, and the hydrogel layer folds from 0° to 180°. The GFe/PDMS layer refers to previous research and has excellent adhesion performance and service life. The double-layered biomimetic surface has both infrared-responsive and dynamic attachment-detachment characteristics. By adjusting the dosage of different NIPAM and BIS, the prepared hydrogel layer has the best driving effect. Optimize the thickness and distribution location of [p(AAm-*co*-NIPAAm-*co*-TA)-Fe], GFe/PDMS and pure PDMS, we designed a single-side irradiation adjusted four-arm gripper, which can grasp an object in about 120s and release it in about 60s. The proposed double-layered biomimetic surfaces in this work have broad applications in the field of intelligent adhesion system and flexible arm grippers to response to infrared environment, perhaps in terms of structure, it provided new insights for designing bionic soft machines [31–38], flexible arms [39].

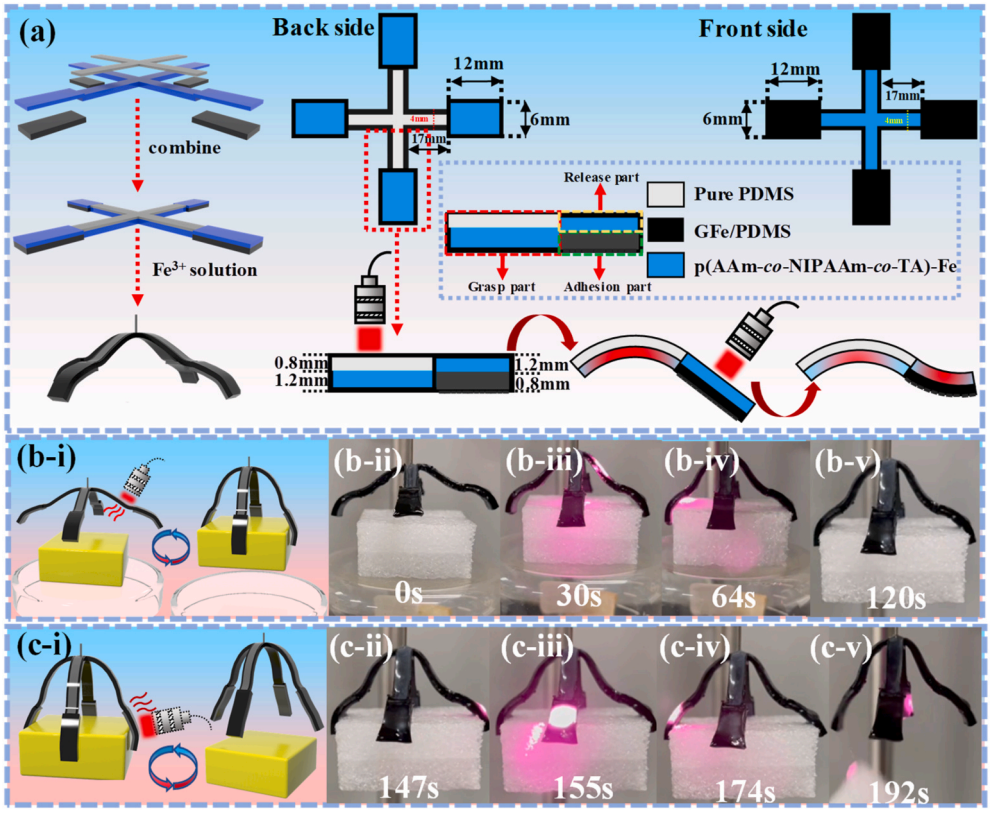

Fig. 4. (a) Adjusted four-arm gripper structure schematic (b) i-v grasp object, (c) i-v release object.

4. Materials, experimental methods and characterization

4.1. Materials

AAm(Acrylamide, AR, 99%), NIPAAm(N-Isopropylacrylamide, contains stabilizer MEHQ, 98%), BIS(N,*N*-Methylenebisacrylamide, 99%), Irga2959(2-(Hydroxymethyl)-N-Methylbenzamide, ≥98%(HPLC)), TA (Tannic Acid, ACS), BP(Benzophenone, 99%), Fe_3O_4 (Iron Oxide, 99%), $FeCl_3{\cdot}6H_2O$ (AR, 99%),1,4-Dioxane(ACS, ≥99%), were purchased by Aladdin(Shanghai, China). PDMS(Polydimethylsiloxane) was purchased by Dow Corning(U.S.A). Glass plates and tape can be purchased at any market.

4.2. Experimental method

1. Preparation of p(AAm-*co*-NIPAAm-*co*-TA)-Fe monolayer driving layer hydrogel: The preparation method refers to the previous reports and has been improved[25]. In Short, AAm, NIPAAm and TA were used as main body to prepare precursor solution (Table 1 for specific parameters). The main body were fully mixed and transferred to a container composed of two glass plates (1 mm apart). After UV light curing for 5 min, the container was removed to form p(AAm-*co*-NIPAAm-*co*-TA). p(AAm-*co*-NIPAAm-*co*-TA) was immersed in different concentrations of iron ion solution for 30min-1h to ensure the full combination of Fe^{3+} and the driving layer hydrogel to form p (AAm-*co*-NIPAAm-*co*-TA)-Fe. Then p(AAm-*co*-NIPAAm-*co*-TA)-Fe was immersed in distilled water for 1 h to replace iron ion solution.
2. Preparation of p(AAm-*co*-NIPAAm) -based hydrogels: The specific operation of precursor solution based on AAm, NIPAAm are shown in the preparation method of p(AAm-*co*-NIPAAm-*co*-TA)-Fe.
3. Preparation of PDMS biomimetic gecko surface: Preparation method of PDMS biomimetic gecko surface is shown in priorpaper [16]. Simply put, PDMS precursor solution and cross-linking agent were mixed in a mass ratio of 10: 1, and different proportions of Fe_3O_4 magnetic nanoparticles were added to the mixture, and the bubbles in the liquid were removed by vacuum pumping. Then poured into silicon template with micro-array structure activated by trimethylchlorosilane. After drying at 70 °C for 30 min, a stable PDMS membrane was formed, which was carefully ripped off from one side until the PDMS membrane was completely detached from the template.
4. Preparation of dual-arm gripper and four-arm gripper: Firstly, the silicon template (4 cm * 4 cm) was fixed on the glass (5 cm * 5 cm), and the VHB double-sided adhesive with 1 mm thickness was adhered around the glass. The PDMS-Fe_3O_4 precursor was slowly dropped to make it fully spread, and a uniform magnetic field was applied above it for 5 min. Then transferred to 70 °C oven curing 30 min. Cooling to room temperature, the prepared samples were transferred to benzophenone solution and soak for 10min. Then the upper surface was encapsulated by glass slide and added into p(AAm-*co*-NIPAAm-*co*-TA) precursor solution. The p(AAm-*co*-NIPAAm-*co*-TA) was cured under UV light for 5–10 min to make p(AAm-*co*-NIPAAm-*co*-TA) glue. Then the cured [p(AAm-*co*-NIPAAm-*co*-TA)]-GFe/PDMS was removed from the glass and soaked in a certain concentration of ferric chloride solution for 1 h, and then removed and soaked in distilled water for 1 h. Then the surgical knife was used to cut into the desired shape such as two arms and four arms grabbers.
5. Preparation of adjusted four-arm gripper: Firstly, 0.8 mm thick VHB tape was bonded around the first 8 cm * 8 cm glass plate, and some PDMS precursor was poured. Curing in 70 °C oven for 30 min, after curing, the prepared samples were cut into width of 4 mm, length of 17 mm cross shape; the second 8 cm * 8 cm glass plate was bonded with 1.3 mm thickness VHB tape, and fixed part of the silicon template (silicon template thickness 0.5 mm), pouring part of the PDMS-Fe_3O_4 precursor, and uniform magnetic field was added above the samples for 5min, transferred to 70 °C oven to cure for 30min. The PDMS and GFe/PDMS with multiple arrays of microstructure were cut off and soaked in 15% mass ratio of BP solution for 10 min. Then, it was taken out and washed twice with anhydrous ethanol, and the multiple arrays of xylene on the surface were removed. The VHB tape with 2.5 mm thickness was adhered around a glass plate again, and the other treated glass plate was carefully aligned on the VHB tape. The p(AAm-*co*-NIPAAm-*co*-TA) precursor was added into the encapsulated glass and cured for 5 min. The p(AAm-*co*-NIPAAm-*co*-TA) precursor was peeled off from the packaging container and soaked in 0.5 mol/L ferric chloride solution for 1 h, and then the p (AAm-*co*-NIPAAm-*co*-TA)-Fe was soaked in distilled water for 1 h to replace the iron ion solution. Cutting multiple positions with a scalpel. Then adjusted four-arm gripper were formed.

4.3. Characterization

1. Hydrogel test of p(AAm-*co*-NIPAAm-*co*-TA)-Fe driving layer: UV–visible spectrophotometer (SHIMAZU UV-2600) was used to measure the absorbance between 200 and 900 nm. Fourier transform infrared spectrometer (Thermo Scientific Nicolet iS10FTIR Spectrometer, U.S.A, Wavenumber range 400-4000 cm^{-1}, SNR50000: 1, 32 scan times) and Raman spectrometer (Thermo Scientific DXR2 Raman Imaging Microscope, U.S.A, Continuous laser beam $\lambda = 785$ nm, test range 400–3100 cm^{-1}, cumulative scan 5 times, object environment 50 times, power 5 mW, integration time 50s) were used to test the functional groups. XPS (Thermo Scientific ESCALAB 250Xi, U. S. A, Monochromatic AlKa ($h\nu = 1486.6$ eV)) was used.
2. Surface adhesion test of gecko-like toe PDMS surface: Scanning probe microscope (AFM Dimension Icon, U.S.A) was used to test the adhesion of the gecko-like toe PDMS surface to ensure that the surface of the sample was not destroyed. A polystyrene ball with a diameter of about 10 μm was modified on the tipless probe as the probe tip, the cantilever is made of silicon; and the type is NANOSENSORS, TL-FM-50; S/N: 85815F13L1419.
3. Shear force test on the gecko-like toe PDMS surface: platform with a fixed pulley was assembled to prepare a glass plate. The plastic beaker and lead were fixed on one side of the glass, and the other side adhered to the bionic gecko surface, and 20 g preload pressure was added above the gecko-like toe PDMS surface.

Credit author statement

Xiaohang Luo, Conceptualization, Methodology, Validation, Data curation, Writing-original draft, Writing-review and editing, Visualization. Xiaoxiao Dong, Conceptualization, Data curation, Writing-original Draft, Writing-review and editing. Hong Zhao, Supervision. Travis Shihao Hu, Writing-review and editing, Supervision. Xiuping Lan, Visualization, Investgation. Lan Ding, Visualization, Resources. Jiapeng Li, Visualization. Huiqin Ni, Visualization. Jordan A. Contreras, Visualization. Hongbo Zeng, Supervision. Quan Xu, Conceptualization, Supervision.

Declaration of competing interest

The authors declare that they have no known competing financial interests or personal relationships that could have appeared to influence the work reported in this paper.

Data availability

No data was used for the research described in the article.

Acknowledgments

This work was supported by the National Natural Science Foundation

of China (No. 52211530034, No. 51875577), Natural Sciences and Engineering Research Council of Canada (NSERC), the Canada Research Chairs Program, the National Natural Science Foundation of China (No. 51575528), the Science Foundation of China University of Petroleum-Beijing (No. 2462020XKJS01), and the U.S. National Science Foundation (Award No. 2004251).

The authors (Xiaoxiao Dong, No. 202006440137; No. 201908530039) would like to acknowledge the support by China Scholarship Council.

Appendix A. Supplementary data

Supplementary data to this article can be found online at https://doi.org/10.1016/j.mtphys.2022.100919.

References

[1] P.F.A. Maderson, Keratinized epidermal derivatives as an aid to climbing in gekkonid lizards, Nature 203 (1964) 780–781, https://doi.org/10.1038/203780a0.
[2] C. Holland, A.E. Terry, D. Porter, F. Vollrath, Comparing the rheology of native spider and silkworm spinning dope, Nat. Mater. 5 (2006) 870–874, https://doi.org/10.1038/nmat1762.
[3] H. Chen, P. Zhang, L. Zhang, H. Liu, Y. Jiang, D. Zhang, Z. Han, L. Jiang, Continuous directional water transport on the peristome surface of Nepenthes alata, Nature 532 (2016) 85–89, https://doi.org/10.1038/nature17189.
[4] H. Peisker, J. Michels, S.N. Gorb, Evidence for a material gradient in the adhesive tarsal setae of the ladybird beetle Coccinella septempunctata, Nat. Commun. 4 (2013) 1661, https://doi.org/10.1038/ncomms2576.
[5] X. Gao, L. Jiang, Water-repellent legs of water striders, Nature 432 (2004), https://doi.org/10.1038/432036a, 36-36.
[6] K. Autumn, Y.A. Liang, S.T. Hsieh, W. Zesch, W.P. Chan, T.W. Kenny, R. Fearing, R. J. Full, Adhesive force of a single gecko foot-hair, Nature 405 (2000) 681–685, https://doi.org/10.1038/35015073.
[7] Y. Tian, N. Pesika, H. Zeng, K. Rosenberg, B. Zhao, P. McGuiggan, K. Autumn, J. Israelachvili, Adhesion and friction in gecko toe attachment and detachment, Proc. Natl. Acad. Sci. U. S. A 103 (2006) 19320–19325, https://doi.org/10.1073/pnas.0608841103.
[8] Q. Xu, Y. Wan, T.S. Hu, T.X. Liu, D. Tao, P.H. Niewiarowski, Y. Tian, Y. Liu, L. Dai, Y. Yang, Z. Xia, Robust self-cleaning and micromanipulation capabilities of gecko spatulae and their bio-mimics, Nat. Commun. 6 (2015) 8949, https://doi.org/10.1038/ncomms9949.
[9] X. Li, P. Bai, X. Li, L. Li, Y. Li, H. Lu, L. Ma, Y. Meng, Y. Tian, Robust scalable reversible strong adhesion by gecko-inspired composite design, Friction 10 (2022) 1192–1207, https://doi.org/10.1007/s40544-021-0522-4.
[10] Y. Song, J. Yuan, L. Zhang, Z. Dai, R.J. Full, Size, shape and orientation of macro-sized substrate protrusions affect the toe and foot adhesion of geckos, J. Exp. Biol. 224 (2021) jeb223438, https://doi.org/10.1242/jeb.223438.
[11] W.R. Hansen, K. Autumn, Evidence for self-cleaning in gecko setae, Proc. Natl. Acad. Sci. U. S. A 102 (2005) 385–389, https://doi.org/10.1073/pnas.0408304102.
[12] H. Hu, D. Wang, H. Tian, Q. Huang, C. Wang, X. Chen, Y. Gao, X. Li, X. Chen, Z. Zheng, J. Shao, Bioinspired hierarchical structures for contact-sensible adhesives, Adv. Funct. Mater. 32 (2022) 2109076, https://doi.org/10.1002/adfm.202109076.
[13] S. Baban Navajit, A. Orozaliev, S. Kirchhof, J. Stubbs Christopher, Y.-A. Song, Biomimetic fracture model of lizard tail autotomy, Science 375 (2022) 770–774. https://doi/10.1126/science.abh1614.
[14] K. Autumn, M. Sitti, A. Liang Yiching, M. Peattie Anne, R. Hansen Wendy, S. Sponberg, W. Kenny Thomas, R. Fearing, N. Israelachvili Jacob, J. Full Robert, Evidence for van der Waals adhesion in gecko setae, Proc. Natl. Acad. Sci. U. S. A 99 (2002) 12252–12256, https://doi.org/10.1073/pnas.192252799.
[15] S. Singla, D. Jain, M. Zoltowski Chelsea, S. Voleti, Y. Stark Alyssa, H. Niewiarowski Peter, A. Dhinojwala, Direct evidence of acid-base interactions in gecko adhesion, Sci. Adv. 7 (2021): eabd9410. https://doi/10.1126/sciadv.abd9410.
[16] X. Dong, R. Zhang, Y. Tian, M.A. Ramos, T.S. Hu, Z. Wang, H. Zhao, L. Zhang, Y. Wan, Z. Xia, Q. Xu, Functionally graded gecko setae and the biomimics with robust adhesion and durability, ACS Appl. Polym. Mater. 2 (2020) 2658–2666, https://doi.org/10.1021/acsapm.0c00282.
[17] Z. Wang, Slanted functional gradient micropillars for optimal bioinspired dry adhesion, ACS Nano 12 (2018) 1273–1284, https://doi.org/10.1021/acsnano.7b07493.
[18] Q. Liu, D. Tan, F. Meng, B. Yang, Z. Shi, X. Wang, Q. Li, C. Nie, S. Liu, L. Xue, Adhesion enhancement of micropillar array by combining the adhesive design from gecko and tree frog, Small 17 (2021): 2005493, https://doi.org/10.1002/smll.202005493.
[19] X. Luo, X. Dong, Y. Hou, L. Zhang, P. Zhang, J. Cai, M. Zhao, M.A. Ramos, T.S. Hu, H. Zhao, Q. Xu, Photo-detachable self-cleaning surfaces inspired by gecko toepads, Langmuir 37 (2021) 8410–8416, https://doi.org/10.1021/acs.langmuir.1c00568.
[20] Y. Mi, Y. Niu, H. Ni, Y. Zhang, L. Wang, Y. Liu, M.A. Ramos, T.S. Hu, Q. Xu, Gecko inspired reversible adhesion via quantum dots enabled photo-detachment, Chem. Eng. J. 431 (2022): 134081, https://doi.org/10.1016/j.cej.2021.134081.
[21] S. Ma, D. Wang, Y. Liang, B. Sun, S.N. Gorb, F. Zhou, Gecko-inspired but chemically switched friction and adhesion on nanofibrillar surfaces, Small 11 (2015) 1131–1137, https://doi.org/10.1002/smll.201402484.
[22] Y. Zhang, S. Ma, B. Li, B. Yu, H. Lee, M. Cai, S.N. Gorb, F. Zhou, W. Liu, Gecko's feet-inspired self-peeling switchable dry/wet adhesive, Chem. Mater. 33 (2021) 2785–2795, https://doi.org/10.1021/acs.chemmater.0c04576.
[23] S.W. Taylor, D.B. Chase, M.H. Emptage, M.J. Nelson, J.H. Waite, Ferric ion complexes of a DOPA-containing adhesive protein from Mytilus edulis, Inorg. Chem. 35 (1996) 7572–7577, https://doi.org/10.1021/ic960514s.
[24] H. Fan, J. Wang, Q. Zhang, Z. Jin, Tannic acid-based multifunctional hydrogels with facile adjustable Adhesion and cohesion contributed by polyphenol supramolecular chemistry, ACS Omega 2 (2017) 6668–6676, https://doi.org/10.1021/acsomega.7b01067.
[25] X. Zhang, L. Chen, C. Zhang, L. Liao, Robust near-infrared-responsive composite hydrogel actuator using Fe^{3+}/tannic acid as the photothermal transducer, ACS Appl. Mater. Interfaces 13 (2021) 18175–18183, https://doi.org/10.1021/acsami.1c03999.
[26] T. Yamashita, P. Hayes, Analysis of XPS spectra of Fe^{2+} and Fe^{3+} ions in oxide materials, Appl. Surf. Sci. 254 (2008) 2441–2449, https://doi.org/10.1016/j.apsusc.2007.09.063.
[27] C.D. Wagner, L.H. Gale, R.H. Raymond, Two-dimensional chemical state plots: a standardized data set for use in identifying chemical states by x-ray photoelectron spectroscopy, Anal. Chem. 51 (1979) 466–482, https://doi.org/10.1021/ac50040a005.
[28] M. Chai, W. Tong, Z. Wang, Z. Chen, Y. An, Y. Zhang, Piezoelectric-Fenton degradation and mechanism study of Fe_2O_3/PVDF-HFP porous film drove by flowing water, J. Hazard Mater. 430 (2022): 128446, https://doi.org/10.1016/j.jhazmat.2022.128446.
[29] Y. Yu, H. Yuk, G.A. Parada, Y. Wu, X. Liu, C.S. Nabzdyk, K. Youcef-Toumi, J. Zang, X. Zhao, Multifunctional "hydrogel skins" on diverse polymers with arbitrary shapes, Adv. Mater. 31 (2019): 1807101, https://doi.org/10.1002/adma.201807101.
[30] H. Li, Y. Liang, G. Gao, S. Wei, Y. Jian, X. Le, W. Lu, Q. Liu, J. Zhang, T. Chen, Asymmetric bilayer CNTs-elastomer/hydrogel composite as soft actuators with sensing performance, Chem. Eng. J. 415 (2021): 128988, https://doi.org/10.1016/j.cej.2021.128988.
[31] Q.L. Zhu, C. Du, Y. Dai, M. Daab, M. Matejdes, J. Breu, W. Hong, Q. Zheng, Z. L. Wu, Light-steered locomotion of muscle-like hydrogel by self-coordinated shape change and friction modulation, Nat. Commun. 11 (2020) 5166, https://doi.org/10.1038/s41467-020-18801-1.
[32] X. Wang, B. Yang, D. Tan, Q. Li, B. Song, Z.-S. Wu, A. del Campo, M. Kappl, Z. Wang, S.N. Gorb, S. Liu, L. Xue, Bioinspired footed soft robot with unidirectional all-terrain mobility, Mater. Today 35 (2020) 42–49, https://doi.org/10.1016/j.mattod.2019.12.028.
[33] X. Yang, Y. Chen, X. Zhang, P. Xue, P. Lv, Y. Yang, L. Wang, W. Feng, Bioinspired light-fueled water-walking soft robots based on liquid crystal network actuators with polymerizable miniaturized gold nanorods, Nano Today 43 (2022): 101419, https://doi.org/10.1016/j.nantod.2022.101419.
[34] A.H. Gelebart, D. Jan Mulder, M. Varga, A. Konya, G. Vantomme, E.W. Meijer, R.L. B. Selinger, D.J. Broer, Making waves in a photoactive polymer film, Nature 546 (2017) 632–636, https://doi.org/10.1038/nature22987.
[35] Z. Sun, Y. Yamauchi, F. Araoka, Y.S. Kim, J. Bergueiro, Y. Ishida, Y. Ebina, T. Sasaki, T. Hikima, T. Aida, An anisotropic hydrogel actuator enabling earthworm-like directed peristaltic crawling, Angew. Chem. Int. Ed. 57 (2018) 15772–15776, https://doi.org/10.1002/anie.201810052.
[36] H. Shahsavan, A. Aghakhani, H. Zeng, Y. Guo, S. Davidson Zoey, A. Priimagi, M. Sitti, Bioinspired underwater locomotion of light-driven liquid crystal gels, Proc. Natl. Acad. Sci. U. S. A 117 (2020) 5125–5133, https://doi.org/10.1073/pnas.1917952117.
[37] C. Li, A. Iscen, H. Sai, K. Sato, N.A. Sather, S.M. Chin, Z. Álvarez, L.C. Palmer, G. C. Schatz, S.I. Stupp, Supramolecular–covalent hybrid polymers for light-activated mechanical actuation, Nat. Mater. 19 (2020) 900–909, https://doi.org/10.1038/s41563-020-0707-7.
[38] M. Yang, Y. Xu, X. Zhang, H.K. Bisoyi, P. Xue, Y. Yang, X. Yang, C. Valenzuela, Y. Chen, L. Wang, W. Feng, Q. Li, Bioinspired phototropic MXene-reinforced soft tubular actuators for omnidirectional light-tracking and adaptive photovoltaics, Adv. Funct. Mater. (2022) 2201884, https://doi.org/10.1002/adfm.202201884.
[39] C.-Y. Lo, Y. Zhao, C. Kim, Y. Alsaid, R. Khodambashi, M. Peet, R. Fisher, H. Marvi, S. Berman, D. Aukes, X. He, Highly stretchable self-sensing actuator based on conductive photothermally-responsive hydrogel, Mater. Today 50 (2021) 35–43, https://doi.org/10.1016/j.mattod.2021.05.008.